Designing High-Power Single-Frequency Lasers

Hans Wenzel

Ferdinand-Braun-Institut für Höchstfrequenztechnik
Albert-Einstein-Str.11, 12489 Berlin, Germany

Introduction

Single-frequency, single-spatial mode distributed feedback (DFB) and distributed Bragg reflector (DBR) lasers have important applications in communication, spectroscopy and frequency conversion. Whereas for InP-based lasers in the 1300nm – 1550nm wavelength range the fabrication of integrated Bragg gratings is well-established using multi-step epitaxial techniques, it is more complicated for shorter-wavelength GaAs-based lasers. The achievement of an output power (P) of more than 100mW is an additional challenge. Here, we well focus on the development of GaAs-based ridge waveguide (RW) DFB lasers emitting below 1μm.

Our group obtained more than 100mW CW output power at 780nm and more than 300mW at 860nm with RW DFB lasers [1][2]. For the achievement of these results, besides an optimised fabrication procedure a carefully modelling of the complete device is necessary. In my talk I will present the major modelling aspects as well as some technological details and experimental results. In this abstract, I will address some selected issues.

Modelling

For the computer-aided design of DFB lasers, we use a hierarchy of different tools which allow a fast, but accurate optimisation. For example, for the basic design of the epitaxial layer structure a one-dimensional optical mode solver is sufficient in order to calculate such parameters as the effective indices, absorption losses, confinement factors, coupling coefficients of Bragg gratings and far field angles. In order to investigate the influence of the substrate in GaAs-based lasers, the mode solver should be able to account both for the real and the imaginary part of the dielectric function [3], which is mostly not possible with mode solvers integrated in commercially available laser simulators.

In order to calculate the lasing behaviour including the stability of the lateral and longitudinal modes, the carrier transport and possibly heat flow and the propagation of the optical field within the cavity have to be modelled. In dependence of the parameters to be optimised, different tools are used. For example, in order to calculate leakage currents over heterojunctions or current spreading and carrier diffusion in laterally structured devices (such as RW lasers), a 2D drift-diffusion simulator is employed. In order to investigate lateral mode stability above threshold

and electrical or thermal roll-over, the drift-diffusion equations must be solved self-consistently with the equations for the optical field and a heat-conduction equation. For that purpose we use the commercially available simulator “WIAS-TeSCA” [4]. On the other hand, for the investigation of the basic dependence of threshold current, external differential efficiency and longitudinal-single mode yield on parameters like cavity length, coupling coefficient and phases of the Bragg grating at the facets, greatly simplified assumptions for the carrier and heat transport can be made [5], which allows a fast scan of the multi-dimensional parameter space.

Figs. 1 and 2 depict some exemplary modelling results for 860nm RW DFB laser. Fig. 1 shows threshold current and slope efficiency in dependence on coupling coefficient and cavity length of a DFB laser with a second order index grating. For high-power lasers, a long cavity with L>1mm is desirable. Hence, the real part of the coupling coefficient should be chosen to κ_r<10cm^{-1}. The discontinuities are related to jumps of the lasing mode from the long-wavelength to the short-wavelength side of the stop band. The κ_r values where the mode jumps occur depend very sensitively on the magnitude of the imaginary part κ_i of the coupling coefficient due to first order radiation, which was assumed to increase with κ_r. It is interesting to note that at the jumps the efficiency rises. However, this fact can hardly be exploited experimentally with a second order index grating because it is very difficult to adjust κ_i experimentally due to its strong dependence on the duty cycle and the shape of the grating.

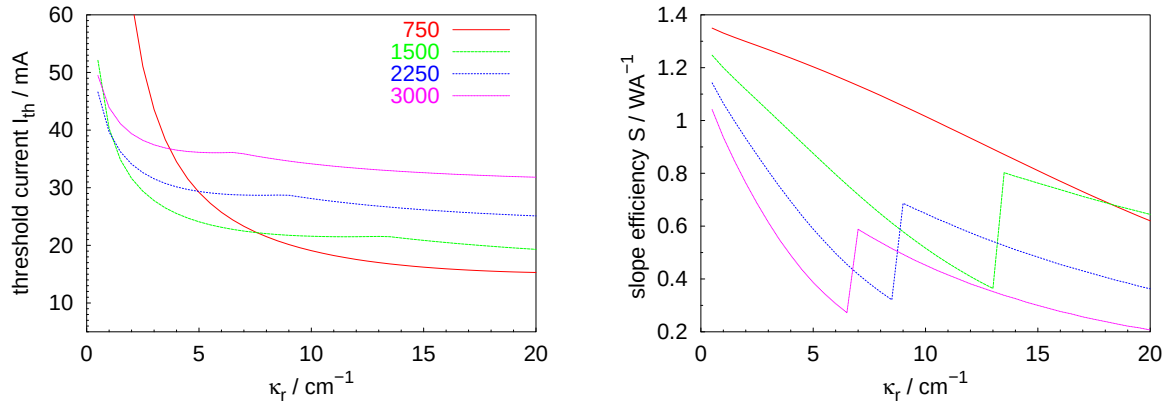

Fig. 1: Calculated threshold current (left) and front facet slope efficiency (right) of a 860nm RW DFB laser versus the real part of the coupling coefficient for different cavity lengths in μm. The imaginary partκ_i is varied as κ_i = – 0.1 κ_r. The reflection coefficients are R_0=0 (front facet) and R_L=0.95 (rear facet).

Fig. 2 shows the influence of the unpredictable phases of the Bragg grating at the facets on the slope efficiency and the lasing wavelength. The slope efficiency can vary from less than 0.8 W/A up to more than 1 W/A (internal losses α_0 = 5 cm^{-1}). Around φ_L = 0.25π, the lasing mode jumps again from the long-wavelength to the short wavelength side of the stop band.

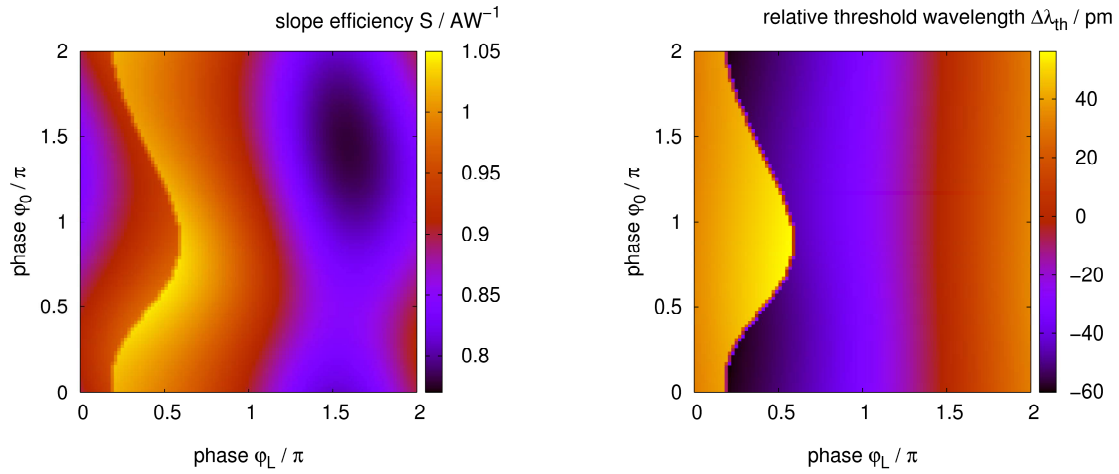

Fig. 2: Calculated color-scale plot of the front facet slope efficiency (left) and relative threshold wavelength (right) versus the phases φ_0 and of φ_L of the grating at the front and rear facets, respectively. The reflection coefficients are $R_0=10^{-3}$ (front facet) and $R_L=0.95$ (rear facet). The coupling coefficient is $\kappa = (5 - i\ 0.5)\ cm^{-1}$.

Device structure, fabrication procedure and experimental results

For lasers emitting in the desired wavelength range, AlGaAs or InGaAsP heterostructures can be employed. Due to the high affinity of aluminium to oxygen, a surface of AlGaAs exposed to air can hardly be overgrown in a conventional metal-organic vapour phase epitaxy (MOVPE) reactor. But on the other hand, the growth of AlGaAs is well established. For these reasons, AlGaAs is employed for the waveguide and cladding layers of the DFB lasers used in this study.

The MOVPE of the structure stops after the growth of a first part of the p-cladding layer and an InGaP/GaAsP/InGaP layer sequence. After the second-order grating has been formed by holographic photolithography and wet-chemical etching into the Al-free layers on top of the wafer, the remaining part of the p-cladding layer and the p-contact layer are grown. The active layer consists of a tensile-strained GaAsP QW (λ=780nm) or a compressively strained InGaAs QW sandwiched between GaAsP spacer layers (λ=860nm). Lateral optical confinement is provided by a 3μm wide ridge-waveguide (RW) with an effective-index step of about $\Delta n_{eff} = 0.003$. The device structure and fabrication procedure is similar to that of the RW Fabry-Perot lasers described in Ref. [6]. Finally, the front and rear facets are anti- and high-reflection coated, respectively. For the CW measurements, the devices are mounted p-side up on AlN submounts and attached to a copper heat sink.

Figs. 3 and Fig. 4 show the experimental power-current characteristics and a mapping of the optical spectrum, respectively, of an optimised device. According to the modelling results of Fig. 1, the cavity length has been chosen to L=1.5mm for an intended real part of the coupling coefficient of $\kappa_r \approx 5cm^{-1}$ in order to obtain a low threshold current and a high efficiency. The maximum output power reaches almost 400mW. Except of a jump of the lasing mode from the shorter to the longer wavelength side of the stop band at I=140mA, there is stable single longitudinal

mode operation over the whole current range. The lateral far field profile shown in the inset in Fig. 3 for an output power of 350mW indicates the high spatial mode purity in addition to the high spectral purity of the lasing emission.

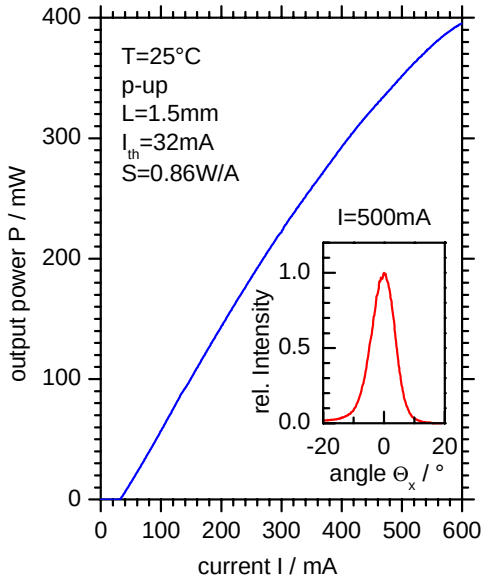

Fig. 3: Experimental power-current characteristics of a 860nm RW DFB laser. Inset: Lateral farfield profile at 350 mW output power.

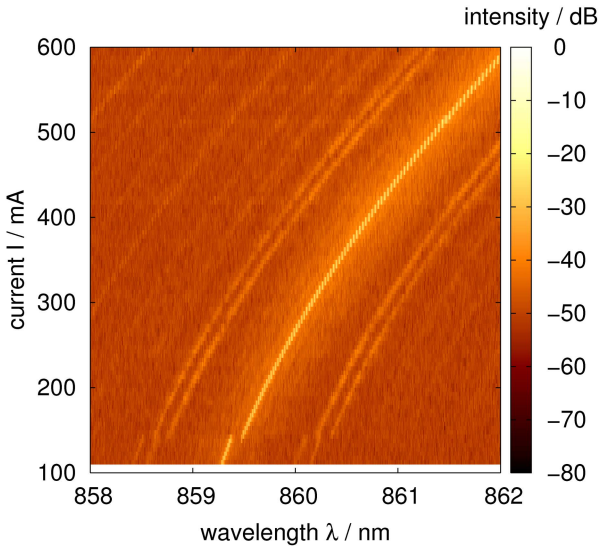

Fig. 4: Measured color-scale plot of the optical intensity versus wavelength and injection current.

Conclusions

Due to the combination of an optimised fabrication procedure and the use of different simulation tools adapted to the respective modelling tasks DFB lasers emitting a record-high single-mode output power at wavelengths below 1 µm were developed.

References

[1] H. Wenzel, M. Braun, J. Fricke, A. Klehr, P. Ressel, G. Erbert and G. Tränkle, Electronics Lett., vol. 38, pp. 1676-1677, 2002.

[2] H. Wenzel, A. Klehr, M. Braun, A. Knauer, B. Sumpf, G. Erbert, H. Schmidt and H.-D. Kronfeldt, CLEO Europe Munich 2002, CI5W, 2002.

[3] H. Wenzel and H.-J. Wünsche, phys. stat. sol. (a), vol. 120, 551-673, 1990.

[4] H. Gajewski et al., Berlin: Weierstrass Institute for Applied Analysis and Stochastics, 2000.

[5] H.-J. Wünsche, U. Bandelow and H. Wenzel, IEEE J. Quantum Electron., vol. 29, pp. 1751-1760, 1993.

[6] G. Beister, F. Bugge, G. Erbert, J. Maege, P. Ressel, J. Sebastian, A. Thies, and H. Wenzel, Electronics Lett., vol. 34, pp. 778-779, 1998.